The Canadian Mineralogist
Vol. 41, pp. 529-540 (2003)

BROMINE IN SCAPOLITE-GROUP MINERALS AND SODALITE: XRF MICROPROBE ANALYSIS, EXCHANGE EXPERIMENTS, AND APPLICATION TO SKARN DEPOSITS

YUANMING PAN[§] AND PING DONG

Department of Geological Sciences, University of Saskatchewan, Saskatoon, Saskatchewan S7N 5E2, Canada

ABSTRACT

Application of an X-ray fluorescence (XRF) microprobe for the analysis of single grains (80 to 1,000 μm in diameter) of Cl-rich minerals for Br has been evaluated for fluorapatite, chlorapatite, scapolite-group minerals (marialite and meonite) and sodalite. A calibration curve based on the Br contents in four international reference materials has been confirmed by measurements on Br-bearing standard solutions and by agreement with the results of Cl-rich minerals from instrumental neutron-activation analyses. Absolute errors associated with individual XRF microprobe analyses (*i.e.*, counting statistics alone) are less than 5%, and the calculated limit of detection in the analysis of single mineral grains is ~1 ppm Br. Matrix and grain-size effects are shown to be negligible. Experiments at 1 atmosphere and 800 to 1000°C yield the following distribution coefficients for Br–Cl exchanges between marialite or sodalite and hydrous NaCl–NaBr melts: $K_D^{marialite–melt} = 0.97 \pm 0.08$ and $K_D^{sodalite–melt} = 0.9 \pm 0.1$. Therefore, the Cl/Br values in marialite and sodalite closely reflect the halogen proportions of their coexisting melts or fluids. The diffusivity of Br in sodalite follows an Arrhenius relation: $D_{Br} = 6.5 \times 10^{-7} \exp(-270 \pm 10 kJ/mol/RT)$ m^2/s, over the temperature range from 800 to 1000°C. D_{Br} in marialite is $1.7 \pm 0.3 \times 10^{-19}$ m^2/s at 800°C. The Cl/Br weight ratios of marialite in the Tieshan Fe skarn deposit, China, cluster around 650 ± 40, supporting an origin involving hydrothermal brines from associated evaporites. Scapolite-group minerals in the exoskarns of the Nickel Plate Au skarn deposit, British Columbia, have Cl/Br from 560 to 570, higher than those (130 to 180) of their counterparts in the endoskarns and vuggy cavities. This variation is attributable to an increased involvement of magmatic water from distal to proximal zones. Similarly, scapolite-group minerals in the Grenville U–Th–Mo–*REE* pegmatite–skarn–vein deposits vary widely in Cl/Br, from 80 to 380, indicative of mixed sources of hydrothermal fluids. This study shows the potential of Br analysis of Cl-rich silicate minerals for constraining the sources and evolution of hydrothermal fluids.

Keywords: XRF microprobe, Br, scapolite-group minerals, sodalite, exchange experiments, distribution coefficient, diffusion coefficient, skarn deposits.

SOMMAIRE

Nous évaluons l'application d'une microsonde à fluorescence X pour l'analyse de grains isolés (de 80 à 1,000 μm de diamètre) pour le Br dans les minéraux porteurs de Cl comme la fluorapatite, la chlorapatite, les minéraux du groupe de la scapolite tels marialite et méionite, et sodalite. Le calibrage a été fait au moyen des teneurs en brome de quatre étalons internationaux, et a été confirmé avec des résultats obtenus pour des solutions standards contenant du Br et des minéraux riches en Cl analysés par activation neutronique instrumentale. Les erreurs absolues associées à une seule analyse par microsonde à fluorescence X, dues aux seules erreurs de comptage, sont inférieures à 5%, et le seuil de détection calculé est d'environ ~1 ppm Br. Les effets de matrice et dus à la taille des grains sont négligeables. Des expériences à 1 atmosphère et entre 800 et 1000°C ont donné les coefficients de distribution suivants pour l'échange Br–Cl entre marialite ou sodalite et un bain fondu hydraté NaCl–NaBr: $K_D^{marialite–bain\ fondu} = 0.97 \pm 0.08$ et $K_D^{sodalite–bain\ fondu} = 0.9 \pm 0.1$. C'est donc dire que le rapport Cl/Br dans la marialite et la sodalite s'approchent étroitement des proportions de ces halogènes dans les bains fondus (ou fluides) coexistants. La diffusivité du Br dans la sodalite répond à une relation de type Arrhenius: $D_{Br} = 6.5 \times 10^{-7} \exp(-270 \pm 10$ kJ/mol/RT) m^2/s, sur un intervalle de température entre 800 et 1000°C. D_{Br} pour la marialite est $1.7 \pm 0.3 \times 10^{-19}$ m^2/s à 800°C. Les valeurs du rapport pondéral Cl/Br de la marialite provenant du gisement de fer de type skarn à Tieshan, en Chine, se regroupent autour de 650 ± 40, et étayent l'hypothèse d'une origine impliquant des saumures issues d'une séquence d'évaporites associée. Les minéraux du groupe de la scapolite des exoskarns du gisement aurifère de Nickel Plate, en Colombie-Britannique, possèdent des valeurs de Cl/Br entre 560 et 570, plus élevées que celles de l'endoskarn et des cavités (entre 130 et 180). Cette variation laisse entrevoir une implication accrue d'une phase fluide orthomagmatique à mesure que l'on s'approche du gisement. De même, dans les minéraux du groupe de la scapolite des pegmatites, skarns et veines à U–Th–Mo–*REE* de la Province du Grenville, le rapport Cl/Br varie beaucoup,

§ *E-mail address*: yuanming.pan@usask.ca

de 80 à 380, indication de sources mixtes des fluides hydrothermaux. Les analyses pour le Br des silicates porteurs de Cl ont le potentiel de cerner la source des fluides hydrothermaux et d'en définir l'évolution.

(Traduit par la Rédaction)

Mots-clés: microsonde à fluorescence X, brome, minéraux du groupe de la scapolite, sodalite, échange par voie expérimentale, coefficient de distribution, coefficient de diffusion, skarn, gisements.

Introduction

Halogens (F, Cl, Br and I) are common constituents in igneous, metamorphic and sedimentary rocks, and are particularly abundant in the hydrosphere. Knowledge of the halogens in geological samples is important in our understanding of magmatic, metamorphic and sedimentary processes (*e.g.*, Sigiura *et al*. 1963, Böhlke & Irwin 1992, Carroll & Webster 1994, You *et al*. 1994, McCaig *et al*. 2000), in the formulation of genetic models for mineral deposits (*e.g.*, Kesler *et al*. 1995, Markl & Piazolo 1998) and in the reconstruction of paleoenvironments (*e.g.*, Channer *et al*. 1997, Siemann & Schramm 2002). There is a considerable body of data on F and Cl in rocks, minerals, melts and fluids (Böhkle & Irwin 1992, Carroll & Webster 1994, and references therein). However, data of Br and I in minerals, except for those in halides (*e.g.*, Stoessell & Carpenter 1986, Raup & Hite 1996), are scarce because of analytical difficulties for these elements (*e.g.*, Heumann *et al*. 1987, Boneß *et al*. 1991, Shinonaga *et al*. 1994, O'Reilly & Griffin 2000).

In this contribution, we report on results of an analysis of Cl-rich minerals for Br by use of an energy-dispersion miniprobe multi-element analyzer [EMMA or X-ray fluorescence (XRF) microprobe; Cheburkin *et al*. 1997]. A major feature of this XRF microprobe is the use of monochromatic X-ray radiation (17.44 keV, Mo$K\alpha$) for excitation, which results in a much lower background than with conventional XRF instruments, and allows the direct analysis of single grains of minerals and solutions for a suite of trace elements (Cheburkin *et al*. 1997). Our main objectives in this study are: 1) to evaluate the application of XRF microprobe for analysis of Cl-rich minerals (including fluorapatite, chlorapatite, marialite and sodalite) for Br, 2) to determine factors controlling the Cl/Br values in scapolite-group minerals and sodalite by ion-exchange experiments, and 3) to document and interpret the Cl/Br values in scapolite-group minerals from selected skarn-type deposits [*i.e.*, the Tieshan Fe deposit, Hubei Province, China: Pan & Dong (1999), the Nickel Plate Au deposit of British Columbia: Pan *et al*. (1994), and the U–Th–Mo–*REE* deposits of the Grenville Province, Ontario and Quebec: Lentz (1992, 1998, and references therein)].

XRF Microprobe, Samples, Analytical Procedures and Experiments

X-ray fluorescence microprobe

The instrument design and operation of the energy-dispersion miniprobe multi-element analyzer (EMMA or XRF microprobe), housed at the University of Saskatchewan (U of SK), have been described in Cheburkin *et al*. (1997). Briefly, the XRF microprobe consists of a conventional 2.0 kW X-ray generator, a concave (Johansson) LiF (220) (R = 250 mm) monochromator, a sample holder attached to a conventional optical microscope, and an energy-dispersion X-ray spectrometer. The spectrometer consists of a 28 mm^2 Si(Li) detector, a pulse amplifier, a 12-bit analogue-to-digital converter and an interface card; it is controlled by an IBM-compatible computer. The X-ray generator is operated at a voltage of 45 kV and a current of 20 mA. The X-ray beam (0.1 $\times$ 2.5 mm) is focused from the LiF monochromator, and is collimated by a conical collimator of 0.2 $\times$ 2.5 mm in dimension. Data acquisition and processing were made on computer programs provided by EMMA Analytical Inc. (Cheburkin *et al*. 1997).

The U of SK XRF microprobe has been calibrated for the following elements: As, Br, Cr, Cu, Fe, Ga, Ge, Hf, Mn, Ni, Rb, Se, Sr, Th, U, and Zn using selected international reference materials (Govindaraju 1994). For example, a calibration curve for Br was established on the basis of four international reference materials (LKSD–1: 11 ppm Br, LKSD–4: 49 ppm, NBS1646: 117 ppm, and MAG–1: 252 ppm; Govindaraju 1994). In this study, a suite of Cl-rich minerals (fluorapatite, chlorapatite, marialite and sodalite, Table 1) from the U of SK reference collection was used to further evaluate this calibration. These minerals, selected on the basis of quantitative electron-microprobe analyses (EMPA) for their homogeneity in Cl and other major elements, were crushed to 100–140 mesh (106–125 μm), and were hand-picked under a binocular microscope to minimize mineral and fluid inclusions. These separates (~0.5 g each) were sent to the Activation Laboratories of Ancaster, Ontario, for instrumental neutron-activation analysis (INAA) for Br. Also, five solutions with 2, 5,

TABLE 1. DESCRIPTION OF MINERAL STANDARDS AND SCAPOLITE-GROUP MINERALS IN SKARN DEPOSITS

Number	Mineral	Location	Description	Ref.
AP-1	fluorapatite	Durango, Mexico	fluorapatite crystals	1
AP-2	chlorapatite	Bob's Lake, Ontario	chlorapatite crystals	1
SCP-1	marialite	Gooderham, Ontario	marialite crystals in a pegmatitic skarn	1*
SCP-2	marialite	Haliburton, Ontario	marialite crystals in skarn	1
SCP-3	marialite	Bancroft, Ontario	marialite crystals in marble	1
SOD-1	sodalite	Bancroft, Ontario	sodalite-rich rock	1
SOD-2	sodalite	Ice River, British Columbia	sodalite-rich rock	1
SOD-3	sodalite	South Africa	sodalite-rich rock	1
99-1-3	scapolite	Tieshan, Daye, Hubei, China	endoskarn	2
99-1-5	scapolite	Tieshan, Daye, Hubei, China	endoskarn	2
99-1-9	scapolite	Tieshan, Daye, Hubei, China	Scp-Cpx endoskarn	2
99-1-12	scapolite	Tieshan, Daye, Hubei, China	Scp endoskarn	2
99-1-14	scapolite	Tieshan, Daye, Hubei, China	Scp-Phl-Cpx-Mt endoskarn	2
99-1-16	scapolite	Tieshan, Daye, Hubei, China	Scp-Phl-Cpx endoskarn	2
99-1-17	scapolite	Tieshan, Daye, Hubei, China	Scp-Phl-Cpx-Grt endoskarn	2
99-1-19	scapolite	Tieshan, Daye, Hubei, China	Scp-Grt-Cpx endoskarn	2
99-1-20	scapolite	Tieshan, Daye, Hubei, China	Scp-Cpx endoskarn	2
99-1-22	scapolite	Tieshan, Daye, Hubei, China	Scp-Cpx endoskarn	2
401-9	scapolite	Nickel Plate, British Columbia	endoskarn	3
401-12	scapolite	Nickel Plate, British Columbia	endoskarn	3
263-13	scapolite	Nickel Plate, British Columbia	exoskarn	3
73-1-8	scapolite	Nickel Plate, British Columbia	exoskarn	3
HD55	scapolite	Nickel Plate, British Columbia	vuggy cavity, Copperfield breccia	3
DL-22B	scapolite	Clark fluorite pegmatite/skarn	Fl-Cpx-Scp-Kfs skarn near pegmatite	4
DL-26A	scapolite	McDonald feldspar pegmatite	Phl-Cpx-Scp-Cc skarn near pegmatite	4
DL-28A	scapolite	Quirk U pegmatite/skarn	Cpx-Scp skarn near pegmatite	4
DL-30A	scapolite	Cardiff North Zone U skarn	Cpx-Scp-Phl-Cc skarn	4
DL-45D	scapolite	Belanger's Corner Zone	Phl-Cpx-Scp skarn	4
DL-60A	scapolite	Matte apatite-U vein	Cpx-Fl-FAp-Cc vein (Scp-Cpx margin)	4
DL-60G	scapolite	Matte apatite-U vein	Cpx-Fl-FAp-Cc vein (Scp-Cpx margin)	4
DL-61A	scapolite	Camp pegmatite/skarn/vein	Phl-Tr-Scp skarn near pegmatite	4
DL-62C	scapolite	Thorianite skarn	Cpx-Phl-Cc skarn	4
DL-66H	scapolite	Calumet U skarn/vein	Py-Phl-Cc-Scp-Cpx skarn near dike	4
DL-70K	scapolite	Litchfield Mo skarn/vein	Ttn-Phl-Scp-Cc skarn vein	4
DL-70N	scapolite	Litchfield Mo skarn/vein	Phl-Scp-Cc skarn	4

Reference: 1 U of Saskatchewan reference mineral collection, 2 Pan & Dong (1999), 3 Pan *et al.* (1994), 4 Lentz (1992). Mineral abbreviations: Cc calcite, Cpx clinopyroxene, FAp fluorapatite, Fl fluorite, Grt garnet, Kfs K-feldspar, Phl phlogopite, Py pyrite, Scp scapolite-group minerals (undifferentiated), Tr tremolite, and Ttn titanite. *: sample SCP-1 is ON8 of Shaw (1960) and Teertstra & Sherriff (1997).

10, 50 and 100 ppm Br were prepared volumetrically from NaBr (Aldrich #22,988–1) and ultra-pure, deionized water, and were analyzed with the XRF microprobe (Table 2).

Samples of scapolite-group minerals from skarn deposits

Details of samples of the scapolite-group minerals from the Tieshan Fe skarn deposit, Hubei Province, China (Pan & Dong 1999), the Nickel Plate Au skarn deposit, British Columbia (Pan *et al.* 1994), and the U–Th–Mo–*REE* deposits of the Grenville Province, Ontario and Quebec (Lentz 1992, 1998) are given in Table 1. Grains of scapolite-group minerals from these skarn deposits were hand-picked from powdered rock samples (Tieshan) or mineral separates (Grenville) under a binocular microscope, and were further examined on a petrographic microscope at high magnifications (250× to 450×) to minimize mineral impurities and fluid inclusions. The Nickel Plate grains were removed from polished thin sections after petrographic observa-

TABLE 2. PRECISION AND ACCURACY OF ANALYSIS FOR Br BY XRF MICROPROBE

		Precision			Accuracy			
Sample	Br ppm	XRFM $n = 6$	SD σ	RSD %	XRFM $n = 16$	SD σ	RSD %	DIFF %
AP-1	8†	7.8	0.8	10.2	7.6	1.2	16	-5.0
AP-2	75	74	4	5.4	64	12	19	-12
SCP-1	42	41	2	4.9	41	2	4.9	-2.1
SCP-2	115	114	5	4.4	114	9	7.9	-1.0
SCP-3	70	75	3	4.0	75	3	4.2	+7.1
SOD-1	234	221	8	3.6	223	11	4.9	-4.7
SOD-2	301	283	11	3.9	284	13	4.6	-5.6
SOD-3	418	395	12	3.0	395	16	4.1	-5.5
Water-1	2‡				2.9	0.2	6.9	+45
Water-2	5				5.6	0.3	5.9	+12
Water-3	10				9.6	0.8	8.3	-4.0
Water-4	50				51	1.9	3.7	+2.0
Water-5	100				107	3.4	3.2	+7.0

† Br contents of mineral separates determined by instrumental neutron-activation analyses; ‡ Br-bearing standard solutions prepared volumetrically from NaBr and deionized water; XRFM: X-ray fluorescence microprobe; SD: standard deviation (one sigma); RSD: relative standard deviation; DIFF: difference.

tions and quantitative EMPA (see below), except that those of sample HD55 were taken directly from single crystals in a vuggy cavity (Pan *et al.* 1994). In general, three grains of scapolite-group minerals from each sample were analyzed with the XRF microprobe. However, 10 grains were examined for sample DL–70K from the Litchfield Mo skarn vein (Table 1), in which a large variation in Br was detected (see below).

Exchange experiments

Eight exchange experiments between minerals and hydrous halide-rich melts were made for a sample of marialite (SCP–1 from Gooderham, Ontario, $Me_{12.2}$: Shaw 1960, Teertstra & Sherriff 1997) and sodalite (SOD–3 from South Africa): using NaCl–NaBr weight ratios of 1:1 and 2:1 and at temperatures of 800 and 1000°C. Each charge, comprising 0.02 g powdered marialite or sodalite grains, 0.08 g NaCl–NaBr mixture and 0.01 g deionized water, was sealed in Au or Pt capsules by welding. The experiments at 800°C, using Au capsules, were performed in a Thermolyne 47900 furnace for 30 days and were quenched in water. The 1000°C experiments in Pt capsules, performed in a Thermolyne 46100 furnace, were planned for 14 days but terminated after 12 days owing to a power failure. The experimental products, after washing with deionized water, were mounted in Pyrex plugs and polished for electron-microprobe analysis.

Electron-microprobe analysis

After the XRF microprobe analysis, the grains of fluorapatite, chlorapatite, scapolite-group minerals (including those from the skarn deposits) and sodalite were mounted on Pyrex plugs, polished and carbon-coated for EMPA, with the exception of scapolite-group minerals from polished thin sections from the Nickel Plate deposit (samples 401–9, 401–12, 263–13 and 73–1–8). These were analyzed by EMPA before their removal. These analyses were performed on a JEOL JXA–8600 Superprobe equipped with three automated wavelength-dispersion and one energy-dispersion spectrometers at the U of SK. Operating conditions included: accelerating voltage 15 kV, beam current 10 nA, beam diameter 5 μm and 20 second counting-time (excepting 60 s for Fe and Sr). Standards included quartz (Si), corundum (Al), diopside (Ca), jadeite (Na), sanidine (K), fayalite (Fe), celestine (Sr), tugtupite (Cl) and anhydrite (S). In addition, marialite ON–70 of Shaw (1960) was used as an independent standard.

Electron-microprobe analyses of ion-exchanged marialite and sodalite were made at an accelerating voltage of 10 kV, a beam current of 10 nA, a beam diameter of ~1 μm, 30 s counting-time, and similar mineral standards as above, except that KBr was added as a standard for Br. The low accelerating voltage was used here to reduce the beam size (see below). Peak-overlap interference between Al and Br was corrected for manually, and was monitored by analyzing a synthetic crystal of end-member $Na_8(Al_6Ge_6)O_{24}Br_2$ (Fleet 1989).

Results and Discussion

Quantitative analysis of Cl-rich minerals for Br by XRF microprobe

Mineral grains selected for XRF microprobe analysis were placed in sample holders made of 4 μm thick Prolene films. Counting times were 10 minutes for typical analyses of single grains, but were increased to 45 minutes for mineral grains that contain less than 10 ppm Br or are smaller than 100 μm in diameter. XRF microprobe analyses of the Br-bearing standard solutions were made on drops in similar sample holders, with counting times of 10 and 45 minutes for Br concentrations above and below 10 ppm, respectively.

Figure 1a shows that the Br contents in fluorapatite, chlorapatite, marialite and sodalite, obtained by the XRF microprobe technique, are in excellent agreement with

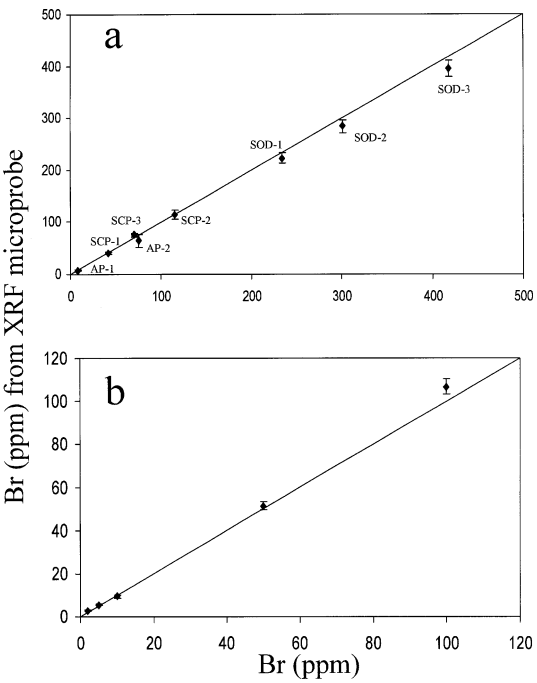

FIG. 1. Comparison of a) Br contents of fluorapatite, chlorapatite, marialite and sodalite obtained from XRF microprobe analysis and instrumental neutron-activation analysis (INAA) (see Table 1 for sample numbers; labeled), and b) Br in standard solutions by XRF microprobe analysis.

those from INAA on bulk mineral separates. The only exception is a large relative standard deviation (19%) of the Br content in chlorapatite from Bob's Lake, Ontario, which is attributable to compositional heterogeneity related to the local presence of small patches of fluorapatite in this sample. Excellent agreement was also obtained for the Br-bearing standard solutions (Fig. 1b).

These results show that the XRF microprobe technique is capable of quantitative analysis of Cl-rich minerals for Br, and that a matrix effect is negligible, at least for the minerals investigated in this study. This lack of a matrix effect is also evident in the successful analysis of the Br-bearing standard solutions (Fig. 1b), which uses the same calibration curve, based on the rock powders. However, a significant matrix effect of this XRF microprobe technique is known for some high-density minerals (*e.g.*, monazite and zircon; Cheburkin *et al.* 1997). Analyses of marialite from sample SCP–3 (Table 1), with grain sizes in the range of 80 to 1,000 μm in diameter, show that a grain-size effect also is negligible.

Precision, accuracy and detection limit

The precision, accuracy and detection limit of the XRF microprobe for the analysis of single mineral grains are all related to a number of variables, such as the grain size and the counting time. For example, the larger the grain size and the longer the counting time, the higher the count rates and the better the counting statistics, respectively, and hence, improved precision and detection limit. The following evaluation of precision, accuracy and detection limit was made for most analyses of mineral grains (*i.e.*, for grains sizes of 100 to 500 μm in diameter and counting times of 10 and 45 minutes for Br concentrations above and below 10 ppm, respectively). This protocol was used to ensure that the absolute errors associated with individual analyses (*i.e.*, counting statistics alone) are less than 5%.

Repeated analyses of selected grains of fluorapatite, marialite and sodalite were used to demonstrate the precision of the XRF microprobe technique (Table 2). Relative standard deviations (RSD) are generally less than 5% for Br concentrations above 10 ppm, but increase to about 10% for concentrations below 10 ppm (Table 2). The accuracy of the XRF microprobe technique has been evaluated by comparison with the INAA results for fluorapatite, chlorapatite, marialite and sodalite (Table 2). The differences between the XRF microprobe and INAA results are <10% for Br concentrations above 10 ppm and 10–20% for concentrations from 2 to 10 ppm (Table 2). The largest difference (+45%), for the standard solution containing 2 ppm Br, may be attributable to significant evaporation because of a counting time of 45 minutes in this analysis. The detection limit (defined as three standard deviations of the background) of the XRF microprobe technique has been established for mineral grains (*i.e.*, a quartz crystal annealed at 1500°C for 12 hours) as well as solution samples, and is approximately 1 ppm Br.

Bromine in Cl-rich minerals

The presence of significant Br in halite and sylvite is well documented (*e.g.*, Stoessell & Carpenter 1986, Berndt & Seyfried 1997). Appel (1997) reported high Br contents (up to 418 ppm) and low Cl/Br values (down to 1.6) in hydrothermally altered Archean komatiitic rocks from West Greenland, and suggested that Br may originally reside in hydroxychlorides (*e.g.*, hibbingite) or in fluid inclusions. It remains unclear whether the trace amounts of Br in nominally anhydrous silicate minerals (*e.g.*, feldspars; Shinonaga *et al.* 1994) are or are not related to the presence of fluid inclusions in these minerals. O'Reilly & Griffin (2000) reported up to 54 ppm Br in fluorapatite from mantle xenoliths by laser ablation – inductively coupled plasma – mass spectrometry (see also Dong & Pan 2002). INAA and XRF microprobe analyses in this study showed that the Durango fluorapatite contains ~8 ppm Br, whereas chlorapatite from Bob's Lake, Ontario, has a notably higher Br content (Table 2).

Scapolite-group minerals and sodalite of this study contain up to 144 and 395 ppm Br, respectively (Tables 2, 3a, b, c). To the best of our knowledge, this is the first report of significant Br in natural Cl-rich aluminosilicates. Bromine is known to strongly partition into aqueous fluids or melts rather than coexisting minerals (Seyfried *et al.* 1986), and in this way is similar to Cl (Carroll & Webster 1994). Therefore, the presence of any fluid inclusions in selected mineral grains could significantly affect the analytical results concerning Br. During the initial stage of this study, anomalously high (and variable) Br contents were encountered in a few grains of halite and were subsequently found to be related to the presence of fluid inclusions. Fortunately, fluid inclusions are generally rare in grains of scapolite-group minerals (Pan *et al.* 1994). Also, care was taken in our selection of the mineral grains to minimize the effect of fluid inclusions and other impurities. On the basis of the mostly homogeneous distribution of Br in scapolite-group minerals, as evidenced by the small standard deviations (Table 3a, b, c), we suggest that the Br contents in scapolite-group minerals and sodalite of this study (Tables 2, 3a, b, c) represent a substitution for Cl in these minerals. This suggestion is supported by a correlation between the Br contents from the XRF microprobe analyses and the Cl contents from EMPA analysis in sample DL–70K (Table 3c).

Results of exchange experiments and factors controlling the Cl/Br values in marialite and sodalite

The experimental products of all four runs on sodalite (Table 4) consist of sodalite, glass and water (at

TABLE 3a. COMPOSITIONS OF SCAPOLITE-GROUP MINERALS FROM THE TIESHAN Fe SKARN DEPOSIT, CHINA

Sample	99-1 -3	99-1 -5	99-1 -9	99-1 -12	99-1 -14	99-1 -16	99-1 -17	99-1 -19	99-1 -20	99-1 -22
SiO_2 wt%	54.5(9)	56.9(7)	52.4(5)	55.0(3)	54.9(4)	58.6(7)	57.8(5)	56.0(4)	55.0(1)	56.2(8)
Al_2O_3	23.8(3)	23.0(3)	24.5(2)	23.5(2)	23.7(4)	22.6(3)	22.8(3)	23.6(2)	23.4(4)	23.0(2)
FeO*	0.16(3)	0.11(4)	0.09(1)	0.12(2)	0.12(1)	0.18(2)	0.14(3)	0.13(2)	0.14(4)	0.13(3)
CaO	8.8(6)	6.8(4)	10.9(3)	8.4(3)	8.5(8)	5.6(4)	6.3(2)	7.9(3)	7.9(9)	7.1(4)
SrO	0.13(2)	0.21(3)	0.07(2)	0.15(3)	0.13(1)	0.09(2)	0.13(2)	0.15(3)	0.10(2)	0.18(2)
Na_2O	8.2(4)	9.2(2)	7.1(1)	8.6(3)	8.3(3)	9.7(4)	9.7(1)	8.6(1)	8.7(4)	9.0(3)
K_2O	0.83(9)	0.7(1)	0.7(1)	0.8(1)	0.6(2)	1.1(2)	0.78(3)	0.77(8)	0.81(5)	0.9(2)
Cl	2.8(1)	3.2(1)	2.20(8)	2.9(1)	2.8(2)	3.72(9)	3.49(2)	3.0(1)	3.0(2)	3.08(8)
SO_3	0.49(4)	0.30(3)	0.51(3)	0.41(4)	0.40(9)	0.35(5)	0.26(3)	0.31(6)	0.30(3)	0.36(6)
CO_2†	1.31	0.97	1.96	1.27	1.33	0.39	0.69	1.25	1.16	1.09
-O=Cl	0.63	0.72	0.49	0.64	0.64	0.84	0.79	0.67	0.68	0.69
Total	100.4	100.6	100.0	100.4	100.1	101.4	101.3	101.1	100.3	100.4
Si *pfu*	7.925	8.130	7.739	7.978	7.956	8.247	8.187	8.013	8.008	8.092
Al	4.075	3.870	4.261	4.022	4.044	3.753	3.813	3.987	3.992	3.908
Fe	0.017	0.012	0.010	0.013	0.013	0.019	0.014	0.014	0.015	0.014
Ca	1.364	1.037	1.727	1.298	1.318	0.843	0.957	1.208	1.227	1.099
Sr	0.011	0.017	0.006	0.013	0.011	0.008	0.011	0.012	0.008	0.015
Na	2.312	2.546	2.020	2.410	2.340	2.637	2.666	2.394	2.443	2.514
K	0.154	0.136	0.139	0.152	0.117	0.193	0.140	0.140	0.150	0.165
Cl	0.686	0.779	0.549	0.703	0.694	0.887	0.839	0.717	0.738	0.753
SO_4	0.054	0.032	0.057	0.045	0.043	0.037	0.028	0.039	0.033	0.033
CO_3	0.261	0.189	0.394	0.252	0.262	0.076	0.133	0.244	0.228	0.214
Me	36	28	44	34	35	23	25	32	32	29
Br ppm	44(8)	68(15)	42(2)	40(0.3)	45(5)	55(2)	54(4)	57(4)	47(8)	50(7)

* total iron as FeO; † calculated on the basis of stoichiometry; *Me*: 100(Ca + Sr)/(Ca + Sr + Na + K); *pfu*: proportion of atom or group per formula unit. Numbers in parentheses are standard deviations (one sigma).

room temperature). Similarly, marialite in experiments at 800°C is well preserved. However, marialite in the two runs at 1000°C (Table 4) broke down completely to form wollastonite and albite. This absence of marialite at 1000°C is consistent with the experimental results of Rebbert (1995), who suggested that marialite is not stable at temperatures above ~900°C (see also Pan 1998). Moreover, the angular morphologies of the prismatic grains of sodalite from all four experiments and the marialite grains from the 800°C runs suggest that dissolution and reprecipitation were negligible in these experiments.

The grains of sodalite and marialite from these experiments contain a thin Br-rich rim (~1 to ~6 μm wide) around the original (unaffected and Br-poor) cores (Fig. 2). With the exception of grains that have well-developed fractures or cleavages, the Br-rich rim on both sodalite (Fig. 2) and marialite is essentially uniform in width. The concentration profiles of Br across these Br-rich rims and the unaffected cores (*e.g.*, Fig. 3) have been obtained by EMPA traverses. Note that the Br-rich rims on marialite and sodalite from the 800°C experiments are less than 2 μm wide. Therefore, the Br profiles across these rims (Fig. 3b) are constructed from average of six EMPA traverses.

The Br concentration profiles of marialite and sodalite (Fig. 3) have been fitted to a non-steady-state diffusion equation for constant concentrations of Br at the surface:

TABLE 3b. COMPOSITIONS OF SCAPOLITE-GROUP MINERALS FROM THE NICKEL PLATE Au SKARN DEPOSIT, BRITISH COLUMBIA

	401-9	401-12	263-12	73-1-8	HD55
SiO_2 wt%	52.6(1)	52.4(4)	50.8(2)	53.5(2)	50.4(5)
Al_2O_3	23.8(1)	24.0(1)	26.0(1)	24.5(1)	24.9(3)
FeO*	0.15(2)	0.18(3)	0.15(1)	0.06(1)	0.08(1)
CaO	11.6(1)	11.6(2)	12.1(2)	9.6(1)	12.8(6)
SrO	0.07(1)	0.04(1)	0.01(1)	0.04(1)	0.06(1)
Na_2O	6.68(8)	6.63(2)	6.2(1)	8.20(4)	5.8(4)
K_2O	0.82(4)	0.78(3)	1.14(2)	0.85(4)	0.84(9)
Cl	1.99(9)	1.94(3)	1.73(4)	2.55(6)	1.7(2)
SO_3	0.02(2)	0.02(1)	0.00(1)	0.02(1)	0.02(2)
CO_2†	2.46	2.53	2.80	1.85	2.79
-O=Cl	0.45	0.44	0.39	0.58	0.38
Total	99.7	99.7	100.6	100.6	99.0
Si *pfu*	7.828	7.636	7.524	7.799	7.586
Al	4.172	4.362	4.533	4.213	4.414
Fe	0.019	0.022	0.019	0.000	0.001
Ca	1.852	1.917	1.927	1.503	2.068
Sr	0.006	0.004	0.001	0.000	0.005
Na	1.927	1.905	1.779	2.318	1.682
K	0.156	0.148	0.215	0.158	0.161
Cl	0.501	0.486	0.434	0.630	0.425
SO_3	0.002	0.002	0.000	0.002	0.002
CO_2	0.497	0.512	0.566	0.368	0.573
Me	47	45	51	40	53
Br ppm	114(6)	108(7)	31(4)	45(3)	128(9)

* total iron as FeO; † calculated on the basis of stoichiometry; *Me*: 100(Ca + Sr)/(Ca + Sr + Na + K); *pfu*: proportion of atom or group per formula unit. Numbers in parentheses are standard deviations (one sigma).

TABLE 3c. COMPOSITIONS OF SCAPOLITE-GROUP MINERALS FROM THE GRENVILLE U–Th–Mo–*REE* DEPOSITS, ONTARIO AND QUEBEC

	DL-22B	DL-26A	DL-28A	DL-45D	DL-60A	DL-60G	DL-61A	DL-62C	DL-66H	DL-70N	DL-70K[a]	DL70K[b]
SiO_2 wt%	52.7(5)	50.7(2)	51.1(4)	58.4(4)	52.4(5)	53.5(3)	43.2(9)	50.6(6)	54.7(4)	47.9(5)	49.9(3)	52.(1)
Al_2O_3	24.4(2)	25.0(2)	24.9(5)	22.4(1)	24.2(3)	24.11)	29.3(5)	25.1(2)	23.2(2)	26.1(5)	25.4(1)	24.4(1)
FeO*	0.09(4)	0.05(2)	0.06(3)	0.01(1)	0.08(2)	0.09(2)	0.02(1)	0.03(1)	0.13(3)	0.04(3)	0.06(2)	0.06(1)
CaO	11.1(3)	12.9(1)	12.0(3)	6.9(4)	11.3(5)	10.6(1)	19.1(3)	12.7(4)	8.73(8)	14.9(4)	13.7(1)	10.8(9)
SrO	0.12(2)	0.16(2)	0.16(4)	0.03(3)	0.25(2)	0.26(2)	0.39(3)	0.29(4)	0.22(4)	0.24(6)	0.19(2)	0.25(1)
Na_2O	6.9(1)	6.0(1)	6.3(2)	8.7(4)	6.7(3)	6.9(2)	2.4(2)	6.0(3)	7.9(1)	4.7(3)	5.44(9)	7.1(8)
K_2O	1.08(9)	0.44(4)	0.94(5)	1.0(1)	1.01)	0.98(6)	0.07(3)	0.58(6)	1.01(8)	0.70(5)	0.56(6)	0.82(2)
Cl	2.06(8)	1.19(3)	1.7(1)	3.3(1)	1.8(1)	1.97(5)	0.20(3)	1.5(1)	2.45(3)	1.0(1)	1.24(6)	2.0(4)
SO_3	0.18(4)	1.51(7)	1.2(1)	0.01(2)	1.11)	1.10(1)	1.8(1)	1.1(1)	0.53(8)	1.68(4)	1.6(1)	1.0(3)
CO_2	2.32	2.56	2.19	1.20	2.09	1.95	3.51	2.41	1.68	2.63	2.46	1.88
-O=Cl	0.46	0.27	0.38	0.73	0.41	0.44	0.05	0.34	0.55	0.23	0.28	0.46
Total	100.5	99.8	100.2	101.3	100.5	101.1	99.9	100.0	100.0	99.6	100.3	100.5
Si *pfu*	7.763	7.630	7.623	8.265	7.765	7.837	6.663	7.579	8.000	7.312	7.503	7.751
Al	4.237	4.370	4.377	3.735	4.235	4.163	5.337	4.421	4.000	4.688	4.497	4.249
Fe	0.002	0.001	0.002	0.001	0.008	0.010	0.003	0.004	0.014	0.003	0.007	0.007
Ca	1.748	2.075	1.918	1.043	1.794	1.669	3.154	2.039	1.368	2.430	2.201	1.710
Sr	0.011	0.014	0.013	0.002	0.019	0.022	0.035	0.025	0.018	0.021	0.017	0.022
Na	1.963	1.751	1.824	2.391	2.001	1.946	0.719	1.741	2.244	1.385	1.586	2.020
K	0.203	0.085	0.180	0.183	0.210	0.184	0.014	0.111	0.189	0.137	0.118	0.155
Cl	0.514	0.303	0.426	0.767	0.459	0.488	0.053	0.381	0.607	0.259	0.317	0.507
SO_3	0.020	0.171	0.128	0.001	0.119	0.122	0.207	0.126	0.058	0.137	0.178	0.115
CO_2	0.466	0.526	0.446	0.232	0.423	0.390	0.740	0.493	0.335	0.549	0.505	0.378
Me	45	53	49	29	45	44	81	52	36	62	56	44
Br ppm	108(11)	31(3)	144(15)	104(13)	78(2)	70(5)	25(5)	91(13)	112(5)	93(1)	70(5)	127(14)

* total iron as FeO; † calculated on the basis of stoichiometry; *Me* = 100(Ca + Sr)/(Ca + Sr + Na + K); a and b, two populations of DL-70K; numbers in parentheses are standard deviations (one sigma).

TABLE 4. SUMMARY OF EXCHANGE EXPERIMENTS

Run #	NaCl/ NaBr	T °C	Time s	Cl/Br†	K_D	D m^2/s	Log D
SCP-1-1	1:1	800	2.59×10^6	0.8 ± 0.1	1.1 ± 0.1	1.98×10^{-19}	-18.70
SCP-1-2	2:1	800	2.59×10^6	1.8 ± 0.1	1.1 ± 0.1	1.48×10^{-19}	-18.83
SCP-1-3	1:1	1000	1.05×10^6				
SCP-1-4	2:1	1000	1.05×10^6				
SOD-3-1	1:1	800	2.59×10^6	0.6 ± 0.1	0.85 ± 0.09	8.13×10^{-20}	-19.09
SOD-3-2	2:1	800	2.59×10^6	1.4 ± 0.1	0.9 ± 0.1	4.13×10^{-20}	-19.38
SOD-3-3	1:1	1000	1.05×10^6	0.6 ± 0.1	0.75 ± 0.09	8.68×10^{-18}	-17.06
SOD-3-4	2:1	1000	1.05×10^6	1.5 ± 0.1	1.0 ± 0.2	4.79×10^{-18}	-17.32

† the surface Cl/Br values (*i.e.*, weight ratios) of marialite and sodalite are based on Cl and Br contents extrapolated from the EMPA traverses (see text for explanation).

$$C_{x,t} = C_0\left[1 - \mathrm{erf}\left(\frac{x}{2\sqrt{Dt}}\right)\right]$$

where $C_{x,t}$ is the concentration of Br at depth x and time t from the surface, C_0 is the surface concentration of Br, and D is the diffusion coefficient in m^2/s (Crank 1975). Here, the surface Cl/Br values of marialite and sodalite cannot be determined directly by EMPA owing to un-

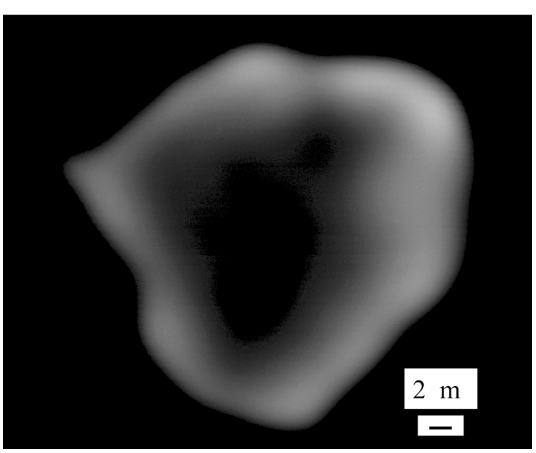

FIG. 2. Back-scattered electron image illustrating a Br-rich rim around the original (Br-poor) core of a sodalite grain from experiment SOD–3–1. Note that the width of the Br-rich rim is fairly uniform.

avoidable edge-effects (*e.g.*, interference from melts and epoxy resin), and hence are extrapolated from the concentration profiles (Fig. 3).

The estimated diffusion-coefficients of Br in sodalite and marialite are given in Table 4. The Br diffusivity in these minerals appears to have a compositional dependence, *i.e.*, increase in D with increasing surface concentrations of Br at a given temperature (Table 4). Also, the D values of Br in marialite and sodalite at 800°C are similar. A least-squares fit to the data from the sodalite experiments (Table 4, Fig. 4) yields an Arrhenius relation: $D = 6.5 \times 10^{-7} \exp(-270 \pm 10 \text{ kJ/mol/RT}) \text{ m}^2/\text{s}$, over the temperature range from 800 to 1000°C.

Figure 4 shows that the diffusion rates of Br in marialite and sodalite are significantly lower than those of F–Cl–OH along the *c* axis, broadly similar to those of F–Cl–OH parallel to the *a* axis and of Sr, but are much lower than those of Nd (and other rare-earth elements) in the apatite-group minerals (Brenan 1993, Cherniak & Ryerson 1993, Cherniak 2000). The rapid diffusion of F–Cl–OH along the *c*-axis direction in apatite-group minerals has been attributed to the location of these anions in the *c*-axis channels (Brenan 1993). The Cl^- and Br^- ions in scapolite-group minerals and sodalite are located in large cages surrounded by rings of (Al,Si) tetrahedra (Papike & Zoltai 1965, Fleet 1989) and, unlike F–Cl–OH in apatite-group minerals, are not confined to channels. Also, the Br^- ion (1.96 Å) is significantly larger than F^-, OH^- and Cl^- (1.33, 1.37 and 1.81 Å, respectively; Shannon 1976). These differences are most likely responsible for the considerably slower diffusivities of Br in scapolite-group minerals and sodalite than those of F–Cl–OH parallel to the *c* axis in apatite-group minerals.

The relatively rapid rates of diffusion of F–Cl–OH in apatite-group minerals led Brenan (1993) to express caution about the application of the halogen chemistry of these minerals to infer melt/fluid compositions, because of possible modification during subsequent thermal events. Dobson (1973) formulated the closure temperatures (T_C) of slowly diffusing species in mineral grains as follows:

$$T_C = \frac{E_a / R}{\ln\left(\frac{ART_c^2 D_o / a^2}{E_a dT/dt}\right)}$$

where E_a is the activation energy of diffusion, R is the gas constant, D_o is the pre-exponential term, A is a geometric factor, a is the grain radius, and dT/dt is the cooling rate. Ganguly & Tirone (1999) pointed out that Dobson's (1973) formulation is applicable only to minerals that have undergone large extents of diffusion (*i.e.*, even the composition at the core of individual grains is affected). Figure 5 shows that the closure temperatures

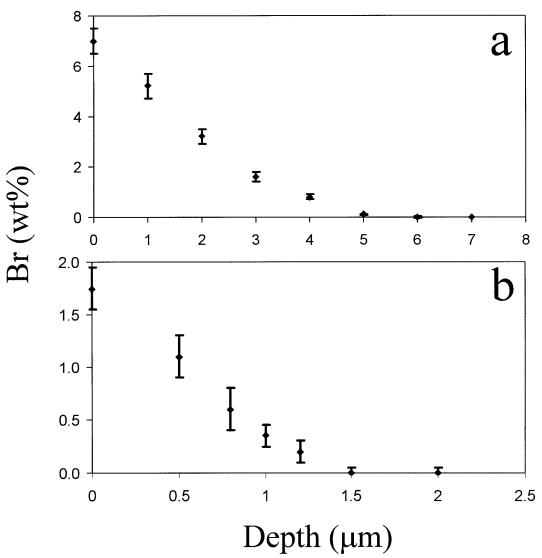

FIG. 3. Representative Br profiles across the rims of: a) marialite of experiment SCP–1–1 (average of spot analyses from six different traverses), and b) sodalite of experiment SOD–3–1. Note that the Br contents at the surface (depth = 0) of mineral grains cannot be determined by EMPA, but are extrapolated from individual traverses.

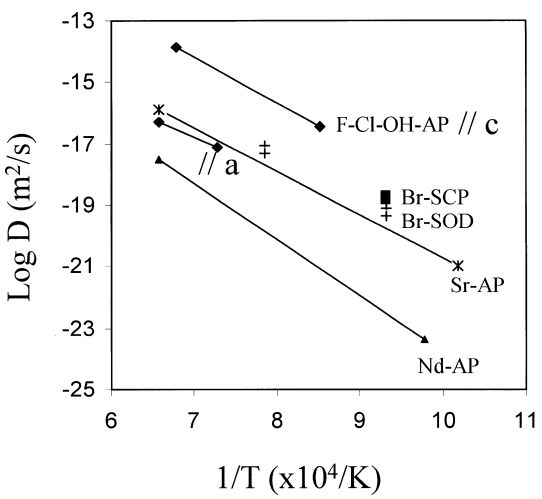

FIG. 4. Arrhenius plot illustrating Br diffusivities in marialite and sodalite. Also shown for comparison are the diffusivities of F–Cl–OH (// *c* and // *a* at 1 atmosphere), Sr and Nd in apatite-group minerals (data from Brenan 1993, Cherniak & Ryerson 1993, Cherniak 2000).

of Br in sodalite are significantly higher than those of F–Cl–OH in apatite-group minerals, but are close to those of Sr in apatite-group minerals. The closure temperatures of Br in marialite are probably similar to those of this element in sodalite, because of similarities in the experimentally determined D_{Br} at 800°C (Table 4) and the structural environments of Br in these minerals.

The Br–Cl exchange between marialite or sodalite and hydrous halide melts can be represented by the following reaction:

$$Br^-_{mineral} + Cl^-_{melt} = Br^-_{melt} + Cl^-_{mineral}.$$

The expression for the distribution coefficient of this exchange equilibrium is:

$$K_D^{mineral–melt} = (X_{Cl}/X_{Br})^{mineral}/(X_{Br}/X_{Cl})^{melt}.$$

The Cl/Br values of the ion-exchanged sodalite at the surface (Fig. 3) are marginally lower than those of the starting materials, giving $K_D^{sodalite–melt}$ from 0.75 ± 0.09 to 1.0 ± 0.1 (Table 4; average 0.9 ± 0.1). The Cl/Br values of the ion-exchanged marialite at the surface are similar to those in the starting materials, yielding $K_D^{marialite–melt}$ close to unity (Table 4; average 0.97 ± 0.08). There is no significant difference in the estimated $K_D^{sodalite–melt}$ values from experiments at 800 and 1000°C (Table 4).

These $K_D^{mineral–melt}$ values for marialite and sodalite, resulting in no significant Cl/Br fractionation, are distinct from those for halides (Stoessell & Carpenter 1986, Berndt & Seyfried 1997, Siemann & Schramm 2002) and apatite-group minerals (Dong & Pan 2002), all of which have marked preference for Cl over Br. This approximately equal uptake of Cl and Br by scapolite-group minerals and sodalite is probably attributable to their accommodation in the large structural cages of these framework aluminosilicates (Papike & Zoltai 1965, Fleet 1989). Fleet (1989) successfully synthesized $Na_8(Al_6Ge_6)O_{24}Cl_2$, $Na_8(Al_6Ge_6)O_{24}Br_2$ and $Na_8(Al_6Ge_6)O_{24}I_2$, with the still larger I^- ion (2.20 Å; Shannon 1976) accommodated in the cage of sodium aluminogermanate sodalite.

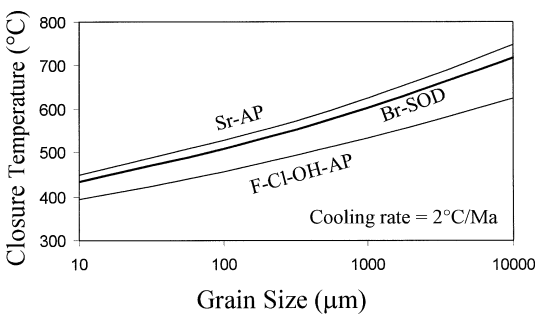

FIG. 5. Closure temperatures for Br in sodalite (Br-SOD, heavy line) as a function of grain sizes at an assumed cooling rate of 2°C/Ma and a spherical geometry, using the formulation of Dobson (1973). Also shown for comparison are values for F–Cl–OH and Sr in grains of apatite-group minerals (F–Cl–OH–AP and Sr–AP, light lines) under similar assumptions (diffusivity data from Brenan 1993, Cherniak & Ryerson 1993).

Application to scapolite-group minerals in skarn deposits

Results of combined EMPA and XRF microprobe analyses of scapolite-group minerals from the Tieshan, Nickel Plate and Grenville deposits (Tables 3a, b, c) are illustrated in Figure 6. Levels of major and minor elements (*e.g.*, Fe, Sr and K) in these samples of scapolite-group minerals are within the ranges in the literature (*e.g.*, Shaw 1960, Teertstra & Sherriff 1997). All samples from the Tieshan deposit are marialite (Me_{23} to Me_{44}), whereas those from the Nickel Plate and Grenville deposits vary from marialite to meonite (Tables 3a, b, c, Fig. 6).

Bromine in scapolite-group minerals of these skarn deposits varies widely, from 25 ppm in a sample of meionite (Me_{81}) to 144 ppm in marialite (Me_{49}; Tables 3a, b, c). The relatively small standard deviations of most samples indicate that Br in scapolite-group minerals is homogeneous in its distribution. However, marialite from sample DL–70K has two populations of different Br and Cl contents (Table 3c). It is noteworthy that their Cl/Br values are similar (Fig. 7), and that the Cl and Br contents both vary with the Al/Si and Na/Ca values, indicative of a crystal-chemical control (Pan *et al.* 1994).

The Cl/Br values of marialite (weight ratio) from the Tieshan deposit cluster around 650 ± 40 (Fig. 7a), whereas those of scapolite-group minerals from the Nickel Plate and Grenville deposits are more variable (Tables 3b, c). In particular, the Cl/Br values of scapolite-group minerals in the Nickel Plate deposit increase from endoskarn (170 to 180) to exoskarn (560 to 570;

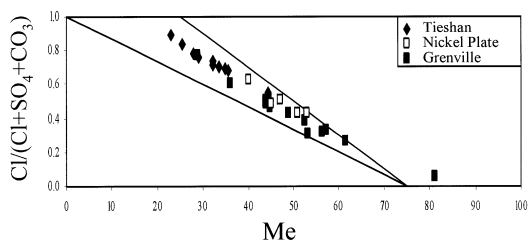

FIG. 6. *X*(Cl) *versus Me* plot illustrating the compositions of scapolite-group minerals from the Tieshan, Nickel Plate and Grenville deposits. *Me*: meionite content.

Table 3b), whereas in the marialite crystals lining cavities in the Copperfield breccia, the Cl/Br value is 130 (Fig. 7a). Scapolite-group minerals in the Grenville deposits reveal a range of Cl/Br values from 80 to 380 (Table 3c, Fig. 7b).

Our exchange experiments have shown that the Cl/Br values in scapolite-group minerals closely reflect those of its coexisting melts or fluids. Therefore, the Cl/Br values of scapolite-group minerals from the skarn deposits are useful in providing constraints on the compositions and sources of ore-forming fluids. For example, the Cl/Br values of marialite in the Tieshan deposit are considerably higher than that of seawater (~280; You *et al.* 1994), but can be explained by the dissolution of halite and sylvite as a mode of origin of the hydrothermal brines (Fig. 7a), providing further support for a genetic model of this deposit involving marine evaporites as country rocks (Pan & Dong 1999). Also, the Cl/Br values of scapolite-group minerals in the exoskarns of the Nickel Plate deposit are close to those of the Tieshan deposit, and may indicate a similar origin. The increase in Cl/Br from endoskarn to exoskarn is readily attributable to an increased involvement of magmatic H_2O in the former. Similarly, the wide variation in Cl/Br in scapolite-group minerals from the Grenville deposits (Fig. 7b) is consistent with varying degrees of mixing of hydrothermal fluids derived from magmatic sources and associated sedimentary rocks (Lentz 1992, 1998).

Finally, there have been numerous applications of Cl/Br systematics from fluid inclusions in constraining the sources and evolution of hydrothermal fluids in a variety of mineral deposits (*e.g.*, Kesler *et al.* 1995). In the present study, we show that the Cl/Br values in Cl-rich minerals are also useful tracers for the compositions and sources of ore-forming fluids, provided that the distribution coefficients of Cl and Br between minerals and coexisting melts and fluids are known. In this respect, scapolite-group minerals and sodalite are special cases in that their Cl/Br values can be used directly as tracers for the sources and evolution of hydrothermal fluids, because their K_D values are close to unity. Another advantage of scapolite-group minerals and sodalite is that the Cl/Br values in these minerals from skarn systems and medium-grade metamorphic terranes are not significantly affected during cooling processes (Fig. 5), unlike those in fluid inclusions.

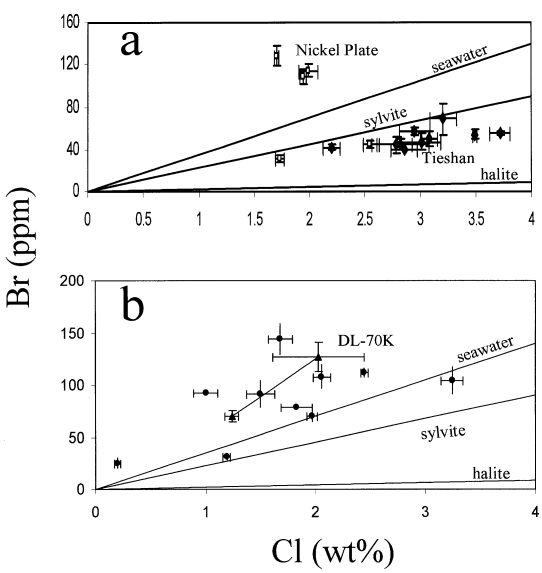

FIG. 7. Br (ppm) *versus* Cl (wt%) plots illustrating scapolite-group minerals from: a) the Tieshan and Nickel Plate skarn deposits, and b) the Grenville pegmatite, skarn, and vein deposits. The reference lines represent the Cl/Br values of seawater, halite and sylvite (data from Stoessell & Carpenter 1986, You *et al.* 1994, Siemann & Schramm 2002).

ACKNOWLEDGEMENTS

We thank C.M. Clark, D.R. Lentz, R.F. Martin, E. Sokolova and an unnamed referee for constructive criticism and many helpful suggestions. We also thank the Saskatchewan Ministry of Economic Development for providing a Strategic Initiative Fund grant for the purchase of the XRF microprobe, A. Cheburkin of the EMMA Analytical Inc. for installation of the XRF microprobe, M.E. Fleet for provision of synthetic $Na_8(Al_6Ge_6)O_{24}Br_2$ crystals and for advice on the crystal structure of sodalite, and D.R. Lentz for provision of samples from the Grenville deposits. Additional financial support for this study was provided by an NSERC research grant.

REFERENCES

APPEL, P.W.U. (1997): High bromine contents and low Cl/Br ratios in hydrothermally altered Archean komatiitic rocks, West Greenland. *Precamb. Res.* **82**, 177-189.

BERNDT, M.E. & SEYFRIED, W.E., JR. (1997): Calibration of Br/Cl fractionation during phase separation of seawater: possible halite at 9° to 10°N East Pacific Rise. *Geochim. Cosmochim. Acta* **61**, 2849-2854.

BÖHLKE, J.K. & IRWIN, J.J. (1992): Laser microprobe analysis of Cl, Br, I, and K in fluid inclusions: implications for sources of salinity in some ancient hydrothermal fluids. *Geochim. Cosmochim. Acta* **56**, 203-225.

BONESS, M., HEUMANN, K.G. & HAACK, U. (1991): Cl, Br and I analyses of metamorphic and sedimentary rocks by isotope dilution mass spectrometry. *Contrib. Mineral. Petrol.* **107**, 94-99.

BRENAN, J. (1993): Kinetics of fluorine, chlorine and hydroxyl exchange in fluorapatite. *Chem. Geol.* **110**, 195-210.

CARROLL, M.R. & WEBSTER, J.D. (1994): Solubilities of sulfur, noble gases, nitrogen, chlorine and fluorine in magmas. *Rev. Mineral.* **30**, 231-279.

CHANNER, D.M.DER., DE RONDE, C.E.J. & SPOONER, E.T.C. (1997). The Cl^-–Br^-–I^- composition of ~3.23 Ga modified seawater: implications for the geological evolution of ocean halide chemistry. *Earth Planet. Sci. Lett.* **150**, 325-335.

CHEBURKIN, A.K. FREI, R. & SHOTYK, W. (1997): An energy-dispersive miniprobe multielement analyzer (EMMA) for direct analysis of trace elements and chemical age dating in single mineral grains. *Chem. Geol.* **135**, 75-87.

CHERNIAK, D.J. (2000): Rare earth element diffusion in apatite. *Geochim. Cosmochim. Acta* **64**, 3871-3885.

_____ & RYERSON, F.J. (1993): A study of strontium diffusion in apatite using Rutherford backscattering spectroscopy and ion implantation. *Geochim. Cosmochim. Acta* **57**, 4653-4666.

CRANK, J. (1975): *The Mathematics of Diffusion* (2nd ed.). Oxford University Press, London, U.K.

DOBSON, M.H. (1973): Closure temperature in cooling geochronological and petrological systems. *Contrib. Mineral. Petrol.* **40**, 259-274.

DONG, PING & PAN, YUANMING (2002): F–Cl–Br partitioning between apatites and halide-rich melts: experimental studies and applications. *Geol. Assoc. Can. – Mineral. Assoc. Can., Program. Abstr.* **27**, A29.

FLEET, M.E. (1989): Structures of sodium alumino-germanates sodalites $[Na_8(Al_6Ge_6O_{24})A_2$, A = Cl, Br, I]. *Acta Crystallogr.* **C45**, 843-847.

GANGULY, J. & TIRONE, M. (1999): Diffusion closure temperature and age of a mineral with arbitrary extent of diffusion: theoretical formulation and applications. *Earth Planet. Sci. Lett.* **170**, 131-140.

GOVINDARAJU, K. (1994): 1994 compilation of working values and sample description for 383 geostandards. *Geostandards Newslett.* **18**.

HEUMANN, K.G., GALL, M. & WEISS, H. (1987): Geochemical investigations to explain iodine-overabundances in Antarctic meteorites. *Geochim. Cosmochim. Acta* **51**, 2541-2547.

KESLER, S.E., APPOLD, M.S., MARTINI, A.M., WALTER, L.M., HUSTON, T.J. & KYLE, J.R. (1995): Na–Cl–Br systematics of mineralizing brines in Mississippi Valley-type deposits. *Geology* **23**, 641-644.

LENTZ, D.R. (1992): *Petrogenesis of U-, Mo-, and REE-bearing pegmatites, skarns, and veins in the Central Metasedimentary Belt of the Southwestern Grenville Province, Ontario and Quebec.* Ph.D. thesis, Univ. of Ottawa, Ottawa, Ontario.

_____ (1998): Late-tectonic U–Th–Mo–REE skarn and carbonatitic vein-dyke systems in the southwestern Grenville Province: a pegmatite-related pneumatolytic model linked to marble melting (limestone syntexis). *In* Mineralized Intrusion-Related Skarn Systems (D.R. Lentz, ed.). *Mineral. Assoc. Can., Short Course* **26**, 519-567.

MARKL, G. & PIAZOLO, S. (1998): Halogen-bearing minerals in syenites and high-grade marbles of Droning Maud Land, Antarctica: monitors of fluid compositional changes during late magmatic fluid–rock interaction processes. *Contrib. Mineral. Petrol.* **132**, 246-268.

MCCAIG, A.M., TRITLLA, J. & BANKS, D.A. (2000): Fluid mixing and recycling during Pyrenean thrusting: evidence from fluid inclusion halogen ratios. *Geochim. Cosmochim. Acta* **64**, 3395-3412.

O'REILLY, S.Y. & GRIFFIN, W.L. (2000): Apatite in the mantle: implications for metasomatic processes and high heat production in Phanerozoic mantle. *Lithos* **53**, 217-232.

PAN, YUANMING (1998): Scapolite in skarn deposits: petrogenetic and geochemical significance. *In* Mineralized Intrusion-Related Skarn Systems (D.R. Lentz, ed.). *Mineral. Assoc. Can., Short Course* **26**, 169-210.

_____ & DONG, PING (1999): The Lower Changjiang (Yangzi/Yangtze River) metallogenic belt, East Central China: intrusion- and wallrock-hosted Cu–Fe–Au, Mo, Zn, Pb, Ag deposits. *Ore Geol. Rev.* **15**, 177-244.

_____, FLEET, M.E. & RAY, G.E. (1994): Scapolite in two Canadian gold deposits: Nickel Plate, British Columbia and Hemlo, Ontario. *Can. Mineral.* **32**, 825-837.

PAPIKE, J.J. & ZOLTAI, T. (1965): The crystal structure of a marialite scapolite. *Am. Mineral.* **50**, 641-655.

RAUP, O.B. & HITE, R.J. (1996): Bromine geochemistry of chloride rocks of the Middle Pennsylvanian Paradox Formation of the Hermosa Group, Paradox Basin, Utah and Colorado. *U.S. Geol. Surv., Bull.* **2000-M**.

REBBERT, C.R. (1995): *Studies of Volatile-Bearing Silicate Minerals: Cl–CO_3 Scapolite Solution Properties and Hydrothermal Oxidation of Synthetic Iron Biotite.* Ph.D. thesis, Univ. Oregon, Eugene, Oregon.

SEYFRIED, W.E., JR., BERNDT, M.E. & JANECKY, D.R. (1986): Chloride depletions and enrichments in seafloor hydrothermal fluids: constraints from experimental basalt alteration studies. *Geochim. Cosmochim. Acta* **50**, 469-475.

SHANNON, R.D. (1976): Revised effective ionic radii and systematic studies of interatomic distances in halides and chalcogenides. *Acta Crystallogr.* **A32**, 751-767.

SHAW, D.M. (1960): The geochemistry of scapolite. II. Trace elements, petrology, and general geochemistry. *J. Petrol.* **1**, 261-285.

SHINONAGA, T., EBIHARA, M., NAKAHARA, H., TOMURA, K. & HEUMANN, K. (1994): Cl, Br and I in igneous standard rocks. *Chem. Geol.* **115**, 213-225.

SIEMANN, M.G. & SCHRAMM, M. (2002): Henry's and non-Henry's law behavior of Br in simple marine systems. *Geochim. Cosmohim. Acta* **66**, 1387-1399.

SIGIURA, T., MIZUTAZI, Y. & OANA, S. (1963): Fluorine, chlorine, bromine, and iodine in volcanic gases. *J. Earth Sci.* (*Nagoya Univ.*) **11**, 272-278.

STOESSELL, R.K. & CARPENTER, A.B. (1986): Stoichiometric saturation tests of $NaCl_{1-x}Br_x$ and $KCl_{1-x}Br_x$. *Geochim. Cosmochim. Acta* **50**, 1465-1474.

TEERTSTRA, D.K. & SHERRIFF, B.L. (1997): Substitutional mechanisms, compositional trends and the end-member formulae of scapolite. *Chem. Geol.* **136**, 233-260.

YOU, C.F., BUTTERFIELD, D.A., SPIVACK, A.J., GIESKES, J.M., GAMO, T. & CAMPBELL, A.J. (1994): Boron and halide systematics in submarine hydrothermal systems: effects of phase separation and sedimentary contributions. *Earth Planet. Sci. Lett.* **123**, 227-238.

Received August 17, 2002, revised manuscript February 25, 2003.